CONF

LBL-13467

Conf-820102--2

Lawrence Berkeley Laboratory
UNIVERSITY OF CALIFORNIA

MASTER

Materials & Molecular Research Division

Presented at the Microstructural Control Conference, Houston, TX, January 18-19, 1982

RESEARCH TOWARD NEW ALLOYS FOR GENERATOR RETAINING RINGS

J.W. Morris, Jr., and K.M. Chang

November 1981

Prepared for the U.S. Department of Energy under Contract W-7405-ENG-48

DISCLAIMER

RESEARCH TOWARD NEW ALLOYS FOR GENERATOR RETAINING RINGS

By

J. W. Morris, Jr. and K. M. Chang*

Materials & Molecular Research Division
Lawrence Berkeley Laboratory

and

Department of Materials Science & Mineral Engineering
University of California, Berkeley

LBL--13467

DE82 011146

* Present address: General Electric Company, Schenectady, N.Y. 12301

This work was supported by the Director, Office of Energy Research, Office of Basic Energy Science, Materials Sciences Division of the U.S. Department of Energy under Contract No. W-7405-ENG-48; and by the Electric Power Research Institute under Contract No. RP 636-2.

MGW

ABSTRACT

The research reported here was undertaken to develop an alloy suitable for use in the retaining rings of two-pole electrical generators that would have three key properties: (1) a yield strength of 200 ksi (1380 MPa) or greater with good residual toughness; (2) resistance to hydrogen embrittlement and stress-corrosion cracking; (3) processability through heat treatment after hot forming, to avoid the ncessity of cold forming of the ring. The principal alloy developed during the course of this work was an iron-based superalloy, designated EPRI-T, which has nominal composition Fe-34.5Ni-5Cr-3Ti-3Ta-0.5Al-1.0Mo-0.3V-0.01B. The alloy is an iron-based superalloy which is strengthened through the formation of cubic γ' precipitates of composition $Ni_3(Ti,Ta,Al)$. When given appropriate aging treatment from the as-forged condition the alloy achieves yield strength in excess of 200 ksi (1380 MPa) with good residual toughness and promising resistance to cracking in gaseous hydrogen and salt water. The composition and processing of the alloy are the result of sequential metallurgical development, the steps of which are described in the body of the paper. The alloy was chosen from a class of iron-based superalloys to achieve high strength in thick sections while maintaining reasonable costs, melting practice, and hot formability. The nickel content of the alloy was adjusted to insure that the alloy would be paramagnetic austenite after aging reaction to form the Ni_3X strengthening precipitates. Tantalum was included among the γ'-forming elements to increase the lattice mismatch of the precipitate and improve alloy strength. Chromium was added to the composition to stabilize the austenite phase and eliminate stress-corrosion cracking susceptibility due to martensitic transformation of the austenite. The Mo-V-B group was included to inhibit intergranular precipitation of the equilibrium η phase and hence suppress a tendency toward intergranular fracture in the alloy.

I. INTRODUCTION

The end turns of the rotor winding of an electrical generator are restrained against centrifugal forces by one-piece retaining rings located at either end of the rotor. These retaining rings are the most highly stressed components of the generator in usual service and are hence of particular structural concern. As a consequence of this concern, the Electric Power Research Institute held a technical workshop in the Fall of 1975 (1) to review the status of retaining ring technology from the materials perspective and to identify present and potential problems. The deliberations of the workshop identified three principal problem areas:

1. Non-magnetic retaining rings for large electrical generators are primarially produced from an Fe-18Mn-5Cr alloy which is cold formed into a high-strength one-piece ring. While materials and manufacturing improvements have led to progressively higher alloy strengths, the current alloy appears to have a maximum useful yield strength below 180 ksi (1242 MPa). This strength is being utilized in current generator designs. Further increases in generator size or winding density will, therefore, require the development of a modified or new high strength alloy.

2. The Fe-18Mn-5Cr alloy is known to be susceptible to stress-corrosion cracking. Enviornmental susceptibility constitutes a potentially serious problem since the retaining rings are exposed to gaseous hydrogen, which is used to cool the generator in most designs, and may also be exposed to moisture, either during operation (in some designs) or during transport and storage prior to installation. The environmental susceptibility of the alloy has, in fact, been implicated in service failures of retaining rings.

3. Cold expanding forged rings of the Fe-18Mn-5Cr alloy is a demanding manufacturing process, but it is essential to establish the needed strength in this or similar alloys. Because of the manufacturing difficulties, the U.S. suppliers of large generator retaining rings withdrew before the early 1970's and there are presently only four suppliers of non-magnetic retaining rings for large electrical generators. Since retaining rings are an essential element of electrical generators, any problem affecting their availability or delivery could have serious consequences for the electric power industry.

The three problems cited by the EPRI workshop would simultaneously be solved if a new alloy were developed which was suitable for use in generator retaining rings, capable of achieving strength levels above 180 ksi (1242 MPa) yield, environmentally insensitive, and formable through forging proceses which could be accomplished by a variety of suppliers. To accomplish this EPRI established an alloy development project at the University of California, Berkeley, (2,3).

The objective of the Berkeley project was to develop an improved retaining ring alloy whose desirable properties could be established through a combination of hot forging and heat treatment without the need for cold deformation. The target properties for the alloy were:

1. The alloy should have an attainable yield strength approaching 200 ksi (1380 MPa).

2. At these strength levels the alloy should have a plane strain fracture toughness (K_{1c}) above 100 ksi $\sqrt{in}$ (110 MPa $\sqrt{m}$), to resist brittle crack

propagation in service.

3. The alloy should remain tough in the presence of gaseous hydrogen and should have good resistance to stress-corrosion cracking in fresh or salt water.

4. The alloy should have low magnetic permeability to minimize leakage flux and electrical losses.

5. The alloy should have whatever other physical, electrical and mechanical properties as required for its use in generator retaining rings.

The most promising class of alloys available for retaining ring alloy development was identified to be the iron-based superalloys, which are austenitic alloys of iron and nickel which are hardened by aging to form a dense distribution of strengthening precipitates. Alloy design research was therefore carried out to develop an appropriate iron-based superalloy. The research was done in three phases: First, a non-magnetic superalloy was developed to have a strength level of 200 ksi (1380 MPa) with good residual toughness after thermal processing from the as-forged condition. This alloy was designated EPRI-E. Second, the environmental properties of the alloy were tested and found to be suspect. In particular, the alloy exhibited a high fatigue crack growth rate when tested in gaseous hydrogen. Metallographic studies suggested that its susceptibility to hydrogen was due to the formation of strain-induced martensite during testing. Third, the alloy was modified chemically to achieve a mechanically stable austenite phase without sacrificing strength or toughness properties. The resulting alloy, designated EPRI-T, appears to satisfy the full set of alloy property requirements.

II. ACHIEVING TARGET STRENGTH AND TOUGHNESS: EPRI-E

The first task of the program was the development of a non-nagnetic iron-based superalloy which could be thermally treated to have yield strength in excess of 200 ksi (1380 MPa) with good residual fracture toughness.

The iron-based superalloys are typically based on the Fe-Ni-Ti ternary alloy system. The alloys are hardened by aging at temperatures in the range 600-800°C to precipitate the ordered cubic γ' (Ni_3Ti) phase. The γ' is an intermediate, metastable precipitate phase, which converts to the hexagonal η phase after long aging time. The equilibrium η phase may also form through a cellular reaction along the grain boundaries. The strength of an iron-based superalloy depends on the inherent strength of the precipitates it contains, i.e., on their resistance to the passage of dislocations, and on the density of the precipitates within the matrix. Both the strength and distribution of the precipitate phase can be controlled metallurgically. The inherent strength of the precipitate depends largely on its composition; the microstructural distribution of precipitates is principally a function of the heat treatment the alloy has received. Both strength and toughness deteriorate if the hexagonal η phase forms.

The magnetic properties of an iron-based superalloy are determined by the matrix composition. To insure paramagnetic behavior, the residual matrix after aging must be fully austenitic and have a nickel content less than approximately 30 wt.%.

A. Alloy Composition.

The composition of the alloy was chosen to accomplish three objectives: To achieve a strong γ' hardening precipitate, to establish a paramagnetic residual matrix, and to inhibit η phase formation at grain boundaries.

The γ' precipitate is a cubic, coherent precipitate which can be cut through by matrix dislocations. Its resistance to the passage of matrix dislocations is the sum of crystallographic and mechanical contributions. The crystallographic resistance has its source in the ordered structure of the precipitate, which has the consequence that a perfect dislocation in the matrix is only a partial dislocation within the supercell of the precipitate. The passage of a dislocation through the precipitate hence introduces a planar fault in the precipitate whose energy of formation must be supplied externally if a dislocation is to cut through. The mechanical resistance has its source in the composition-induced lattice mismatch between the precipitate and the matrix. The associated strain field will interact with the strain field of the dislocation and inhibit its motion.

In theory, the crystallographic contribution to the strength of a γ' precipitate can be increased by choosing its composition so as to increase the energy of formation of the planar faults associated with dislocation passage. However, our current understanding of the inherent properties of the γ' phase does not permit us to do this in an alloy design sense. The mechanical strength of the precipitate will be improved by chemical modifications which increase its lattice mismatch with the parent matrix. The work of Decker and Mihalisin (4) has shown that the lattice parameter of the γ' Ni_3Al phase is strongly modified by the addition of alloy species which substitute for aluminium. The most potent of these is tantalum, which was hence chosen for incorporation in the present alloy. In both iron- and nickel-based superalloys, however, the addition of tantalum has a tendency to transform the structure of the intermediate precipitate from the cubic γ' to the tetragonal γ'' phase (5). In the present alloy the tantalum content

was balanced against titanium with a small admixture of aluminium to assure precipitation of the cubic phase.

The nickel content of the alloy was adjusted to insure a paramagnetic matrix after aging. Since the Fe-Ni binary alloys are both austenitic and paramagnetic over only a narrow composition range, the nickel content was chosen to lie initially in the ferro-magnetic region. It is reduced as the Ni-rich γ' precipitates during aging to yield a residual composition which insures a paramagnetic matrix.

Since the γ' precipitate in an Fe-Ni-based alloy is an intermediate precipitate, equilibrium η phase may form during aging. This phase tends to appear through a cellular reaction along the grain boundaries and has a detrimental influence on alloy toughness. To suppress η phase formation the total hardening element content, Ti + Ta + Al, was held to a reasonably low value. To further improve grain boundary properties a combination of minor elements, Mo, V and B, was added to the alloy in a proportion which is known to have a beneficial effect on grain boundary properties in similar superalloys.

Given these considerations the composition of the alloy, designated EPRI-E, was chosen to be Fe-36Ni-3Ti-3Ta-0.5Al-1.3Mo-0.3T-0.001B.

B. Heat Treatment.

The response of EPRI-E to heat treatment is illustrated in Fig. 1, which shows the development of the γ' phase after aging at 725°C. The γ' appears in a dense distribution of nearly spherical particles which decorate the matrix, as shown in Figs. 1b and 1c. Their crystal structure is given by the diffraction pattern presented in Fig. 1a. The slight displacement of the low index diffraction spots of the precipitate from those of the

matrix document the slight lattice mismatch between the matrix and precipitate phases. This lattice mismatch results in a local elastic strain, which is revealed by the strain contrast in bright field transmission electron microscopic images taken under strong two-beam diffraction conditions (Fig. 1d).

The strength response of the alloy to isothermal aging in the temperature range 500-900°C is shown in Fig. 2. A substantial increase in the hardness was observed after aging at all temperatures between 625 and 800°C. The level of peak hardness and the associated aging time decreases as the aging temperature is raised. The hardening essentially disappears at 900°C, which is apparently above the solvus temperature for the γ' phase.

The results of isothermal aging studies show that the peak hardness lengthens as the aging temperature is lowered, but the required aging time increases dramatically. The kinetics of age-hardening can be improved, and the peak hardness increased by using a "double-aging" heat treatment. In this heat treatment the alloy is first aged to near peak hardness at a temperature high enough to achieve that hardness in reasonable time, and then given a second aging at lower temperature. The hardness response on double-aging is given in Fig. 3, which shows the result of an initial age at 725°C followed by a second aging at 625°C. The dramatic increase in hardness during the second aging treatment is apparent. Microstructural studies show that the increase in hardness during the second aging treatment is due to a secondary precipitation reaction which is induced by the increased supersaturation of the matrix caused by the drop in temperature (Fig. 4). Double-aging is an effective method for achieving high alloy strength in a reasonable total aging time, and yields a dense

distribution of fine precipitate particles.

In all cases the peak level of strength achieved by the alloy is increased and the kinetics of aging are accelerated if the alloy is aged directly from the as-forged condition, without intermediate anneal. This behavior presumably reflects the contribution of matrix defects left over from the forging process.

C. Strength and Toughness Properties.

If alloy EPRI-E is heat treated from the as-forged condition and given a double-aging treatment consisting of 750°C four hours plus 650°C four hours, it develops a yield strength of 205 ksi (1415 MPa) with a plane strain fracture toughness of approximately 105 ksi $\sqrt{in}$ (115 MPa $\sqrt{m}$). These properties meet the strength and toughness goals of the program. They reflect the excellent strength-toughness combination of the alloy when it is processed from the as-forged condition. This strength-toughness characteristic is shown in Fig. 5, and compared with isolated points representing the properties of INCONEL 718 (6) and A-286 (7), which are widely used superalloys. It is also apparent from the figure that the properties of alloy E are less suitable if the alloy is aged after intermediate annealing. An intermediate anneal to remove forging damage leads to a loss in toughness of approximately 20 ksi $\sqrt{in}$ (22 MPa $\sqrt{m}$) at given strength level.

The alloy is paramagnetic in the aged condition.

III. ENVIRONMENTAL RESISTANCE

A. Environmental Testing.

Given that alloy E can be processed to reach or exceed the strength and toughness goals of the program, it must also resist environmental attack. The most important threat is embrittlement in gaseous hydrogen.

To test its resistance to gaseous hydrogen, tensile, notch-tensile, and fatigue crack growth rate studies were conducted on specimens of alloy E which had been processed to yield strengths near 200 ksi (1380 MPa) by double-aging. The tests were conducted in an environmental cell under 0.8 atm. of dry hydrogen.

The tensile tests on the alloy revealed no apparent effect of hydrogen. The yield strength, ultimate tensile strength, and total elongation of the specimens was essentially identical whether they were tested in hydrogen or in air (Table I). Comparative notched tensile tests in hydrogen and air also failed to reveal a consistent effect of the hydrogen atmosphere (Table II). But, although the proportional limit and the ultimate breaking stress were the same in 0.8 atm. hydrogen as they were in air, the plastic extension to ultimate load of the notched tensile specimens was consistently less for the specimens tested in hydrogen, and decreased with the cross-head speed used in the test. While this parameter is not normally measured in notched tensile tests, it did suggest some sensitivity to the presence of hydrogen and prompted studies of the influence of hydrogen on the fatigue crack growth rate, which is believed to be an especially sensitive measure of hydrogen susceptibility (8).

To establish a standard for hydrogen fatigue testing, the fatigue crack growth rate of alloy E was first measured in air. The pre-cracked compact tension fracture toughness specimen was subjected to fatigue, using displacement control to ensure a cyclic crack opening displacement corresponding to a stress intensity at the crack tip which cycled between 0.1 and 0.6 of K_{1c} at a frequency of 1 cycle/sec. In this geometry the maximum load automatically adjusts to ensure a constant crack opening throughout the

test (8), and decreases in proportion to the crack propagation distance. A record of the applied load versus fatigue cycle number was taken at intervals of 500 cycles, and is plotted in Fig. 6. The slope of the curve is proportional to the crack growth velocity.

After the sample had been cycled in air for approximately 4500 cycles, the environmental chamber was evacuated and back filled with 0.8 atm. dry hydrogen. As shown in Fig. 6, the slope of the load-cycle curve immediately changed by a factor of approximately 4.3, indicating a corresponding increase in the fatigue crack growth rate. As a cross check on this result a second specimen was tested under the same conditions but was exposed to 0.8 atm. hydrogen from the beginning of the test. The slope of its load-cycle curve was identical to that of the first specimen when tested in hydrogen. It was concluded from these tests that alloy E is embrittled by hydrogen when it has been heat treated to a high strength level.

B. Metallurgical Analysis.

To explore the metallurgical source of hydrogen embrittlement, fracture surfaces taken from tensile, fracture toughness, and fatigue specimens of alloy E were examined in the scanning electron microscope. The broken surfaces of tensile specimens showed completely ductile rupture. While the fracture toughness specimens all broke in a primarily ductile mode, transgranular quasi-cleavage facets were occasionally noted on the fracture surface. The fatigue fracture surfaces (Fig. 7) failed predominantly in transgranular quasi-cleavage. The fraction of quasi-cleavage was, however, noticeably higher on the fracture surfaces of the specimens fatigued in hydrogen.

Energy dispersive x-ray analysis was used to determine if there was a difference in chemical composition between the cleavage and ductile regions

of the fracture surfaces, but the results were negative. Magnetic measurements, however, showed an increase in magnetic susceptibility in the vicinity of the fracture surfaces which suggested that the transgranular cleavage features represented the fracture of martensite induced by deformation. This deformation-induced martensite was subsequently identified by both x-ray and Mössbauer spectroscopic techniques. Table III shows the results of x-ray diffraction analyses made on various fracture surfaces of alloy E. The percentage of martensite near the fracture surface increased monotonically as the source of fracture changed from overload to fatigue to hydrogen assisted fatigue, in spite of the lower stress intensity employed in the fatigue tests. The morphology of the martensite phase formed near the fracture surface of fracture toughness and fatigue specimens is compared in Fig. 8. In the case of the fracture toughness specimen, martensite plates populate a region below the fracture surface, but do not completely cover the fracture surface itself. In the case of the fatigue specimen the transformed region is much shallower, but the martensite phase forms an almost continuous film along the fracture surface.

The morphological features of the induced martensite phase were somewhat surprising. The fracture toughness specimen was subjected to a higher overall load and would therefore be expected to undergo significant plastic deformation over a region of some depth in the region surrounding the tip of the propagating crack. The martensite would be induced by plastic strain in this region. In the case of fatigue crack growth, the overall load on the specimen is smaller and the propagating crack is quite likely to be sharper, with the consequence that the region of plastic deformation is confined to a narrower volume in the immediate vicinity of the propagating

crack. The unexpected result, which is new in the sense that we were aware of no relevant prior research, is the much greater extent of transformation in the fatigued specimen, and the clear evidence for a hydrogen contribution to the fatigue-induced martensite transformation. The greater fraction of cleavage-type fracture on the hydrogen assisted fatigue surface moreover suggests that the induced phase transformation to a relatively brittle martensite promoted the growth of the fatigue crack, and was responsible for the acceleration of fatigue fracture in the presence of hydrogen.

IV. STABILIZATION OF THE AUSTENITE PHASE: ALLOY EPRI-T.

The results of the environmental tests suggested that an alloy modification which eliminated the deformation-induced martensitic transformation might simultaneously eliminate, or at least substantially decrease, the alloy's slight sensitivity to hydrogen embrittlement. For this reason a modification of EPRI-E was proposed and developed which was altered in composition so as to stabilize the austenite phase against the deformation-induced martensite transformation.

A. Choice of Alloy Composition.

Alloy EPRI-E forms a thermally stable austenite because of its relatively high Ni content. A significant fraction of the Ni is consumed during the precipitation reaction, which forms Ni-rich phases, so it is only the residual Ni composition of the matrix which stabilizes the austenite phase. The allowable Ni content in the matrix is, in fact, bounded from both above and from below for reasons which relate to the magnetic properties of the Fe-Ni binary system. If the residual Ni content is too low, the matrix becomes metastable or unstable with respect to the formation of martensite.

If the residual Ni content is too high then the FCC austenite phase itself becomes ferromagnetic. A reasonably stable nonmagnetic austenite exists only in a narrow composition range near 30 wt.% Ni, and alloy E was developed through a series of rather precise alloy design studies to ensure that the residual Ni content would fall at approximately this level. It hence did not appear feasible to complete the stabilization of alloy E by Ni addition; other stabilizing elements were explored.

Unfortunately, the more common γ stabilizing alloy elements are also unsuitable for the alloy system studied here. Interstitial elements, such as C and N, have a strong affinity for the precipitation hardening elements Ti and Ta and would hence precipitate during heat treatment. The substitutional element Mn is superficially promising but has been reported to decrease the hardening effect when substituted for Ni in Fe-based superalloys (9). Other γ stabilizers, such as Cu, may be promising but have unknown effects on alloys in this composition range.

Chromium, on the other hand, is normally regarded as a ferrite stabilizer, but may be useful in stabilizing the austenite phase in Fe-Ni alloys (10). Its presence in the current alloy offers possible additional benefits since Cr improves oxidation resistance, is believed to improve resistance to other environmental attack, and decreases the Curie temperature of the alloy (the latter effect is the reason why many superalloys are nonmagnetic).

It was therefore decided to test a Cr-modified version of alloy E, which was designated EPRI-T, and given the nominal composition Fe-34.5Ni-5Cr-3Ti-3Ta-0.5Al-1Mo-0.3V-0.1B. Several 20-lb (9.1 kg) ingots were prepared; a typical chemical analysis of alloy composition is shown in Table IV. The

alloy differs from EPRI-E in two respects: it contains a modest 5% Cr addition and it has a slightly lower nickel content. The Cr addition was intended to stabilize the austenite phase. The slight concomitant decrease in Ni was made to compensate for the decrease in Fe due to the Cr addition.

B. Aging Kinetics.

Age-hardening studies were carried out on the Cr-modified alloy T to determine if strength and toughness combinations comparable to those of alloy E could be established. The hardening response of alloy T was found to be quite similar to that of alloy E at all temperatures, which presumably reflects the similarity in precipitate type. However, the precipitation kinetics were relatively slower in alloy T. This modification of the kinetics must be primarily attributed to the presence of Cr, although the slight decrease in the initial Ni concentration may also play a role. The increase in time required to obtain peak hardness in alloy T is shown graphically in Fig. 9, in which the aging time to peak hardness in the two alloys is plotted on a logrithmic scale against the inverse of the aging temperature. The linearity of the relations suggest that the precipitation reaction is thermally activated with a single rate controlling step. The change in composition from alloy E to alloy T causes a shift in the age-hardening curve to longer aging times but does not change the apparent activation energy, which is 67 Kcal per mole in both cases.

Alloy T was also found to have a favorable response to double aging treatments, similar to that previously demonstrated for alloy E. The example curves of alloy hardness during double heat treatment are shown in Fig. 10. The maximum hardnesses obtained in double aged specimens of alloy T were comparable with the highest found in alloy E and suggest that the modified

alloy T is capable of achieving similar strength levels.

C. Strength, Toughness, and Austenite Stability.

To evaluate the influence of the composition modification on the tensile properties of the alloy, examples of alloy E and alloy T were heat treated to similar hardness levels and tested in tension. The stress-strain curves obtained are plotted in Fig. 11 along with changes in magnetic permeability during the tensile test. The speciman of alloy E exhibited a rapid increase in magnetic permeability after yielding, which is caused by the formation of strain-induced martensite. No such increase was found in alloy T. The austenite in this alloy is apparently stable up to fracture; the magnetic susceptibility of the fracture surface was measured at less than 1.01. Presumably as a consequence of the strain-induced martensite transformation, the specimen of alloy E did exhibit a slightly higher tensile strength and a slightly higher plastic elongation before failure.

The measured tensile and fracture toughness data are tabulated in Table V. While the tensile elongation was approximately 25% lower in alloy T than in alloy E, the former alloy still exhibited good ductility compared with that of commercial high strength superalloys. Fracture toughnes measurements disclosed that the two alloys had virtually the same level of toughness.

To obtain a more extended comparison between the strength toughness relations of alloys E and T, the heat treatment of the alloys was systematically varied to yield a variety of strength levels. To continue the curve to higher yield strength, a single specimen of alloy E was given an additional mechanical work prior to aging and brought to a yield strength of 225 ksi (1550 MPa). The fracture toughnesses of these variously treated

specimens were then determined to generate the strength-toughness curves plotted in Fig. 5. Two features of the data should be noted. First, there is virtually no difference between the strength-toughness characteristics of alloys T and E. Second, the strength-toughness data for both alloys divide into two sets depending on whether the alloys were processed from the as-forged (AF) condition or whether they were given an intermediate solution anneal (AN). Alloys processed from the as-forged condition show a consistent strength increment of approximately 20 ksi at the same toughness level. Figure 5 also includes strength-toughness for two commercial superalloys which have previously been suggested as possible candidates for generator rings: INCONEL 718 (6), a nickel-based superalloy, and A-286 (7), an iron-based superalloy. The data show that the experimental tantalum-modified iron-based austenitic alloys developed here exhibit strength-toughness characteristics superior to those of either of the commercial superalloys.

On the basis of the strength and toughness studies, it was concluded that alloy EPRI-T should be processed from the as-forged condition, and that a suitable heat treatment would involve initial aging at 750°C for 8 hrs followed by secondary aging at 670°C for 6 hrs.

After this treatment alloy T had a measured yield strength of 201 ksi (1387 MPa) and ultimate tensile strength of 228 ksi (1573 MPa), a total elongation of 16%, and a tensile reduction in area of 53%. The fracture toughness was measured using full-sized compact tension specimens and was found to be 103 $\sqrt{\text{in}}$ (113 MPa $\sqrt{\text{m}}$). These values meet the target strength-toughness properties for the program.

D. Environmental Resistance.

The environmental resistance of EPRI-T was tested in both gaseous hydrogen and salt water.

To evaluate the hydrogen sensitivity of EPRI-T, notched tensile and pre-cracked compact tension fatigue specimens were tested comparatively in air and hydrogen using specimens heat treated to the fully hardened condition. The results of the test are presented in Table VI and Figs 12 and 13. There was no apparent influence of the 0.8 atm. hydrogen gas on either the notched tensile properties or the fatigue crack growth rate. No magnetic phase was detected on the fracture surfaces of any of these specimens. Scanning electron fractographic studies of the fatigue fracture surfaces showed a similar crack propagation mode in air and hydrogen.

Given the alloy's apparent resistance to gaseous hydrogen, its sensitivity to stress-corrosion cracking in salt water was tested by exposing compact tension specimens 1/2 in. (1.27 cm) thick make from fully hardened plate. The specimens were dead loaded in a 3.5 wt.% aqueous sodium chloride solution to fracture toughnesses in range 40-80 ksi $\sqrt{in}$ (44-88 MPa $\sqrt{m}$) for periods of at least one week. No crack growth was observed in any of the specimens, suggesting that the crack initiation fracture toughness in salt water (K_{1scc}) exceeds 80 ksi $\sqrt{in}$ (88 MPa $\sqrt{m}$).

On the basis of these environmental tests it was concluded that the chromium modification which produced the stable alloy EPRI-T imparted good environmental resistance to both dry hydrogen and salt water. It should be noted, however, that the operating conditions within a hydrogen-cooled generator involve hydrogen pressures of up to 5 atm., in contrast to the 0.8 atm. pressure used in these tests. Further tests are needed to determine compatability with the generator environment.

E. Physical Properties.

A number of physical properties which are relevant to the use of alloy T in generator retaining rings were measured. All measurements on the alloy were in full hardened, double-aged condition. Data are presented in Table VII. The

values obtained are in all cases typical of the known physical properties of commercial Fe-based superalloys.

The only physical parameter which warrants special discussion in terms of the suitability of alloy T for use in generator retaining rings is its coefficient of thermal expansion, which is a relevant property since retaining rings are one-piece forgings which are shrunk-fit onto the generator rotor, generally at ~300°C. The thermal expansion coefficient of alloy T is somewhat below that of the 18Mn-5Cr alloy now in use, which suggests a possible problem if the same shrink-fitting temperature is used. However, alloy T is strengthened by intermetallic precipitates and, consequently, has much greater thermal stability in its yield strength than does the cold-worked 18Mn-5Cr steel. There is no obvious reason why the overall thermal expansion required to seat the retaining ring onto the rotor could not be obtained by heating the retaining ring to a somewhat higher temperature provided the underlying insulation materials retain their properties.

V. CONCLUSION

The results of this work appear sufficient to demonstrate that alloy EPRI-T, Fe-34.5Ni-5Cr-3Ti-3Ta-0.5Al-1Mo-0.3V-0.01B, can be heat treated to satisfy all programmatic requirements for utilization in a thermally processed generator retaining ring. After double aging from the as-forged condition, the alloy obtains a yield strength in excess of 200 ksi (1380 MPa) with a fracture toughness in excess of 100 ksi $\sqrt{in}$ (110 MPa $\sqrt{m}$), is paramagnetic, resistant to environmental attack, and has satisfactory physical properties. These properties were obtained through a systematic, microstructurally based program of alloy development, in which the engineering objectives of the program were translated into a set of suitable criteria on alloy composition and

and microstructure, and the desired microstructure was established through an appropriate combination of composition and processing. Following its laboratory development, the alloy was reported to the Electric Power Research Institute, which has since established a program with the General Electric Company for its further development and evaluation.

The story of this alloy would, however, not be complete without noting a subsidary problem which occurred during the course of the research and has a strong bearing on the commercial viability of the alloy. While the research was in progress the price of the tantalum alloy adddition increased by approximately 400%. Since EPRI-T contains 3 wt.% tantalum, the result was a substantial increase in the projected cost of a finished retaining ring. The reduction or elimination of the tantalum addition to the alloy is hence a high priority objective of the on-going EPRI alloy development project.

ACKNOWLEDGEMENTS

The authors acknowedge contributions to this alloy development project by researchers at the University of California, including Dr. Sungho Jin (now with Bell Telephone Laboratories), Dr. Dale H. Klahn, Dr. J. I. Kim (now with T.J. Watson Research Laboratory, IBM), Dr. J. Koo (now with EXXON Research Laboratories), Professor Gareth Thomas, and personnel of the Electric Power Research Institute including Dr. R. I. Jaffee, Dr. R. Viswanathan, and Dr. K. I. Kinsman (now with Intel Corp.). The authors appreciate helpful discussions with Dr. F. Hull, Dr. J. M. Wells, an others at the Westinghouse Electric Corp., and with Dr. Robert Goldhoff, Dr. Sumio Yukawa, and others at General Electric. This research was supported by the Electric Power Research Institute under contract No. RP 636-2. Preparation of this manuscript was supported by the Director, Office of Energy Research, Office of Basic Energy Sciences, Materials Sciences Division of the U.S. Department of Energy under Contract #W-7405-ENG-48.

Materials Sciences Division of the U.S. Department of Energy under Contract No. W-7405-ENG-48; and by the Electric Power Research Institute under Contract No. RP 636-2.

REFERENCES

1. R. I. Jaffee and R. H. Richman: "A Program of Research on Steel for Utility Applications," EPRI Special Report FP-274-SR, p. 7-1, Electric Power Research Institute, Palo Alto, CA, November, 1976.
2. J. W. Morris, Jr. and G. Thomas: "High Strength Austenitic Alloys for Generator Retaining Rings," EPRI Report FP-1061, Electric Power Research Institute, Pal Alto, CA, April, 1979.
3. K. M. Chang, J. W. Morris, Jr., and G. Thomas: "High Strength Austenitic Alloys for Generator Retaining Rings," EPRI Report CS-1808, Electric Power Research Institute, Palo Alto, CA, April, 1981.
4. R. F. Decker and J. R. Mihalisin: Trans. ASM, 62, 481 (1969).
5. K. M. Chang, J. Y. Koo, J. W. Morris, Jr., and G. Thomas: 37th Ann. Proc. Electron Microscopy Soc. Amer.," 642 (1979).
6. W. A. Logsdon, R. Kossowsky, and J. M. Wells: "Advances in Cryogenic Engineering," vol. 24, p. 197, Plenum Press, New York, 1978.
7. J. M. Wells, W. A. Logsdon, and R. Kossowsky: "Advances in Cryogenic Engineering," vol. 24, p. 150, Plenum Press, New York, 1978.
8. H. G. Nelson: "Hydrogen Embrittlement Testing," ASTM STP 543, p. 152.
9. J. E. Smugeresky: Met. Trans. A, 1977, vol. 8A, p. 1283.
10. K. Ishida and T. Nishizawa: Trans. JIM, vol. 15, p. 217 (1974).

Table I. Hydrogen effect on transversal tensile properties of double-aged Alloy E.

Specimen	Cross Head Speed (m/sec)	Environment	Yield Strength ksi	(MPa)	Tensile Strength ksi	(MPa)	Total Elong. (%)
EH-10	$2.64 \times 10^{-}$	Air	192	(1325)	220	(1518)	14.0
EH-11	$2.64 \times 10^{-}$	H_2 (0.8 atm)	194	(1339)	216	(1490)	5.3*
EH-12	$1.76 \times 10^{-}$	H_2 (0.8 atm)	188	(1297)	215	(1484)	15.0
EH-13	$2.64 \times 10^{-}$	H_2 (0.8 atm)	188	(1297)	214	(1477)	15.0

Table II. Hydrogen effect on notched tensile properties of double-aged Alloy E.

Specimen	Cross Head Speed (m/sec)	Environment	Proportional Limit* ksi	(MPa)	Ultimate Stress* ksi	(MPa)	Plastic Extension to Ultimate Load (10^{-5}m)
EH-1	1.27×10^{-6}	H_2 (0.8 atm)	275	(1898)	304	(2098)	11.4
EH-2	1.27×10^{-6}	Air	272	(1877)	305	(2105)	17.5
EH-3	1.27×10^{-7}	H_2 (0.8 atm)	280	(1932)	303	(2091)	9.1
EH-4	1.27×10^{-6}	Air	278	(1918)	303	(2091)	

* Stress based on actual area at root of notch.

Specimen data: Nominal gauge length - 0.5" -1.27 cm
Nominal gauge diameter - 0.125"-0.3175 cm
Diameter at notch - 0.100"-0.254 cm
Notch angle - 45°

Table III. X-ray diffraction analysis on various fracture surfaces of alloy E.

Phase	Fatigue-H_2	Fatigue-Air	Rapid Fracture
Martensite (%)	86	73	61
Austenite (%)	14	27	39

Table IV. Chemical analysis of alloy T.

Element	Nominal Concentration (wt.%)	Analyzed Concentration (wt.%)
Iron (Fe)	Balance	Balance
Nickel (Ni)	34.5	34.5
Chromium (Cr)	5.0	4.5
Titanium (Ti)	3.0	2.83
Tantalum (Ta)	3.0	2.87
Aluminium (Al)	0.5	0.48
Molybdenum (Mo)	1.0	0.90
Vanadium (V)	0.3	0.3
Boron (B)	0.01	0.01
Carbon (C)	-o-	$\leqslant$0.01

Table V. Mechanical properties of induced-transformed alloy E and Cr-stabilized alloy T.

Alloy Type	Yield Strength ksi	(MPa)	Tensile Strength ksi	(MPa)	Elongation (%)	Reduction in area	Fracture Toughness ksi$\sqrt{in}$	(MPa$\sqrt{m}$)
E	193	(1332)	230	(1587)	24	60	104	(114)
T	195	(1345)	223	(1539)	18	53	105	(115)

Table VI. Results of notched tensile tests of alloy T in air and in hydrogen.

Specimen	Cross Head Speed (m/sec)	Environment	Proportional Limit* ksi	(MPa)	Ultimate Stress* ksi	(MPa)	Plastic Extension to Ultimate Load (10^{-5} m)
TH-1	1.27×10^{-6}	Air	255	(1760)	283	(1953)	12.7
TH-2	1.27×10^{-6}	H_2 (~0.8 atm)	255	(1760)	293	(2022)	12.7

* Stress based on actual area at root of notch.

Specimen data:

Nominal gauge length	- 0.5"	1.27 cm
Nominal gauge diameter	- 0.125"	0.3175 cm
Diameter at notch	- 0.100"	0.254 cm
Notch angle	- 45°	

Table VII. Physical properties of full-hardened alloy T.

Density	8.26 gm/cm^3
Thermal Expansion coefficient	15.8×10^6 in/in°C
Resistivity	72.7 μΩ-cm
Magnetic Susceptibility	≤ 1.01
Elastic Modulus	27.1×10^6 psi 1.87×10^5 MPa

FIGURE CAPTIONS

Figure 1. Transmission electron microscopic images of γ' precipitates in alloy E: (a) selected area diffraction pattern, (001) orientation; (b) bright-field view showing the precipitates in structure contrast; (c) dark-field view from the (100) superlattice reflection; (d) bright-field image under two-beam diffraction conditions, showing the internal strain field.

Figure 2. The change of hardness in alloy E on isothermal aging at various temperatures.

Figure 3. Double-aging hardening curves for alloy E.

Figure 4. The size distribution of γ' precipitates after single aging for 8 hrs at 750°C and after supplementary aging for 8 hrs at 650°C. Secondary precipitation during the second aging gives rise to the high density of small-diameter particles.

Figure 5. The strength-toughness relations for alloys EPRI-E and T processed from the as-forged (AF) and annealed (AN) conditions. The results are compared with isolated data for the superalloys INCONEL 718 and A-286.

Figure 6. Fatigue crack growth curves for pre-cracked specimens of alloy E.

Figure 7. Scanning electron fractographs of faully hardened alloy E fatigued in air and hydrogen.

Figure 8. Etched cross sections of the fracture surfaces of alloy E broken in single loading (fracture toughness test) and by fatigue in air showing the morphology of the deformation-induced martensite.

Figure 9. Aging time to peak hardness for alloys E and T as a function of aging temperature.

Figure 10. The development of hardness during single and double aging of alloy T.

Figure 11. Comparative stress-strain curves for alloys T and E after double aging; the magnetic permeability is also plotted as a function of the strain.

Figure 12. Fatigue crack growth curve for alloy T, showing the hydrogen-insensitivity of the crack growth rate.

Figure 13. Fatigue fractograph of the full-hardened alloy T in (a) air, (b) H_2.

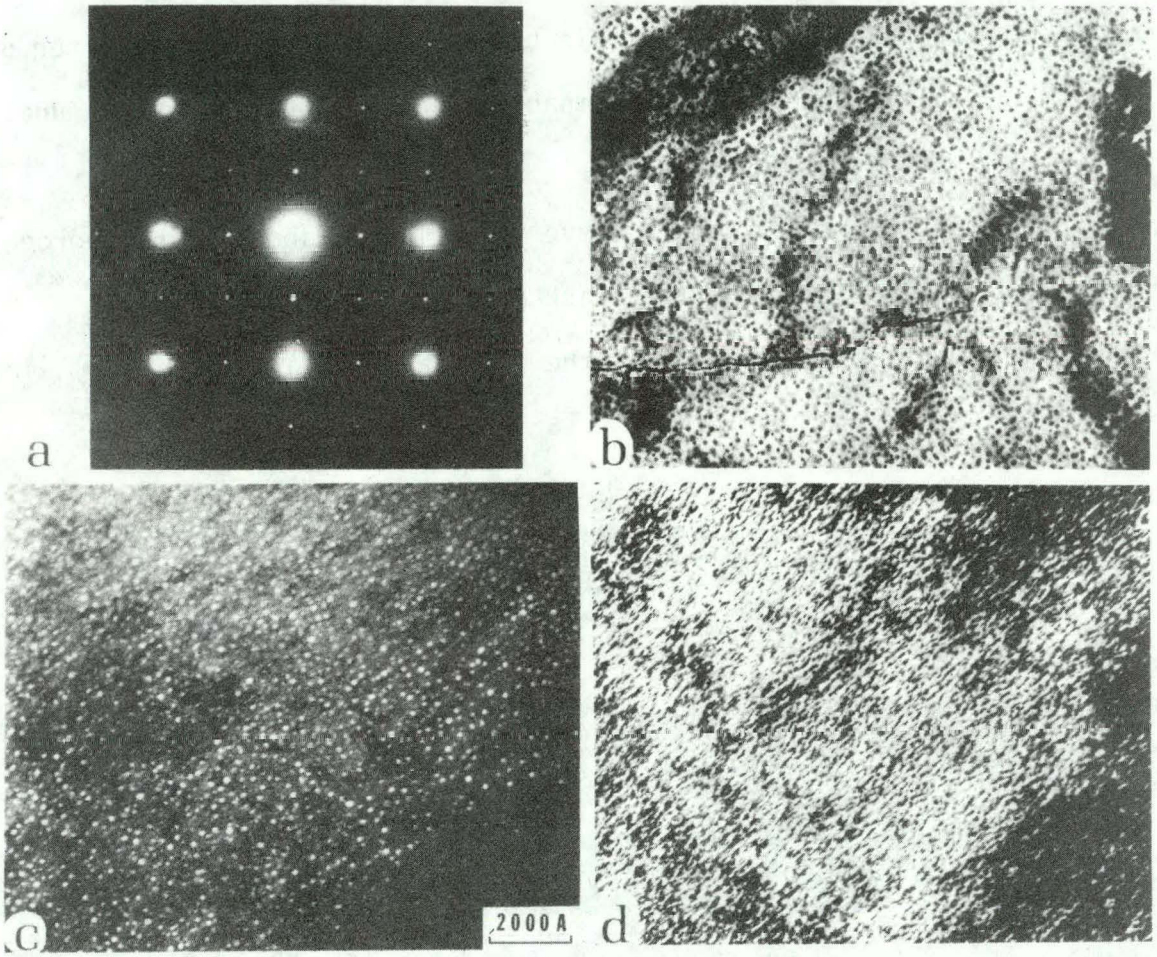

XBB 796-7735

Figure 1

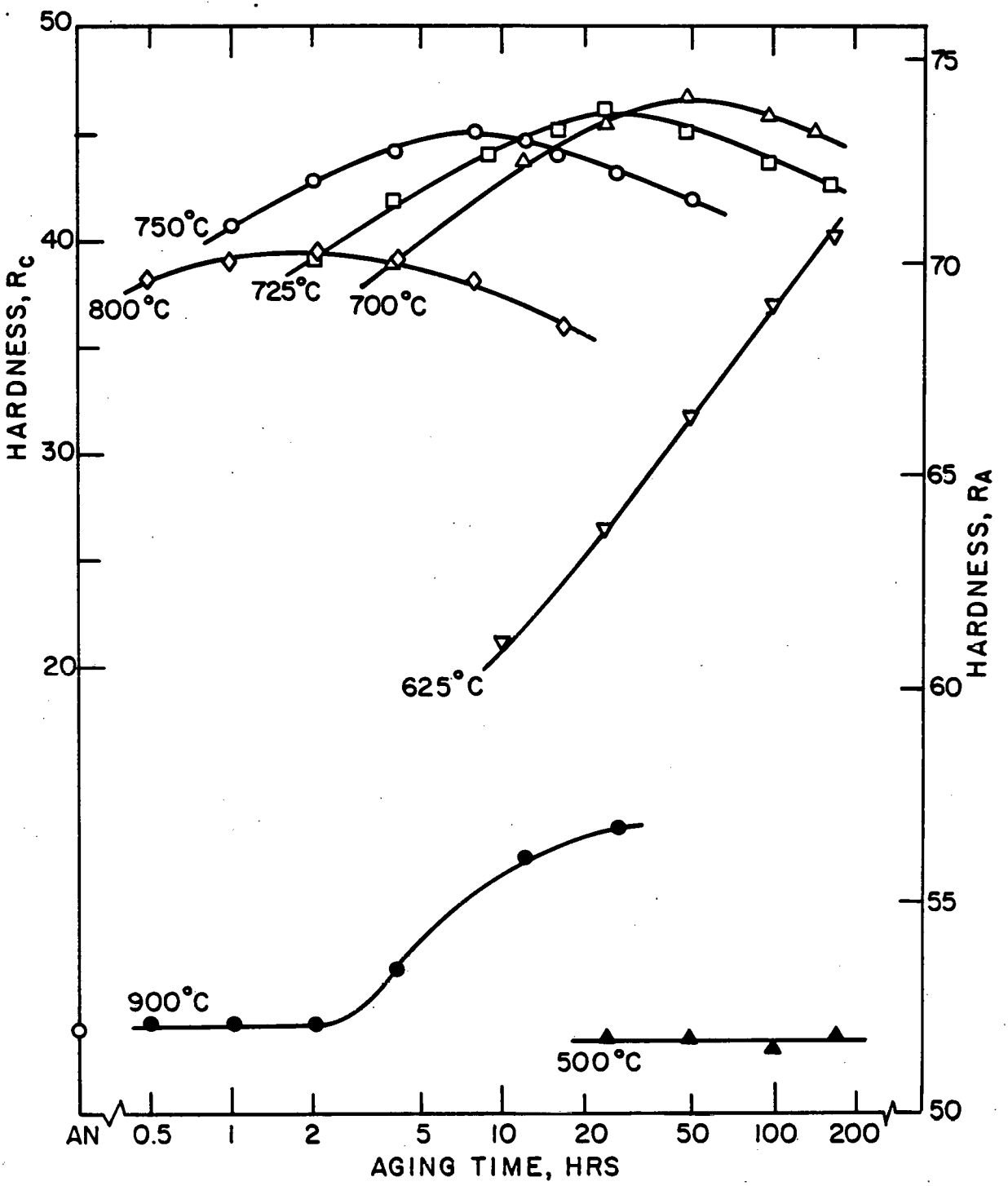

Figure 2

XBL793-5951

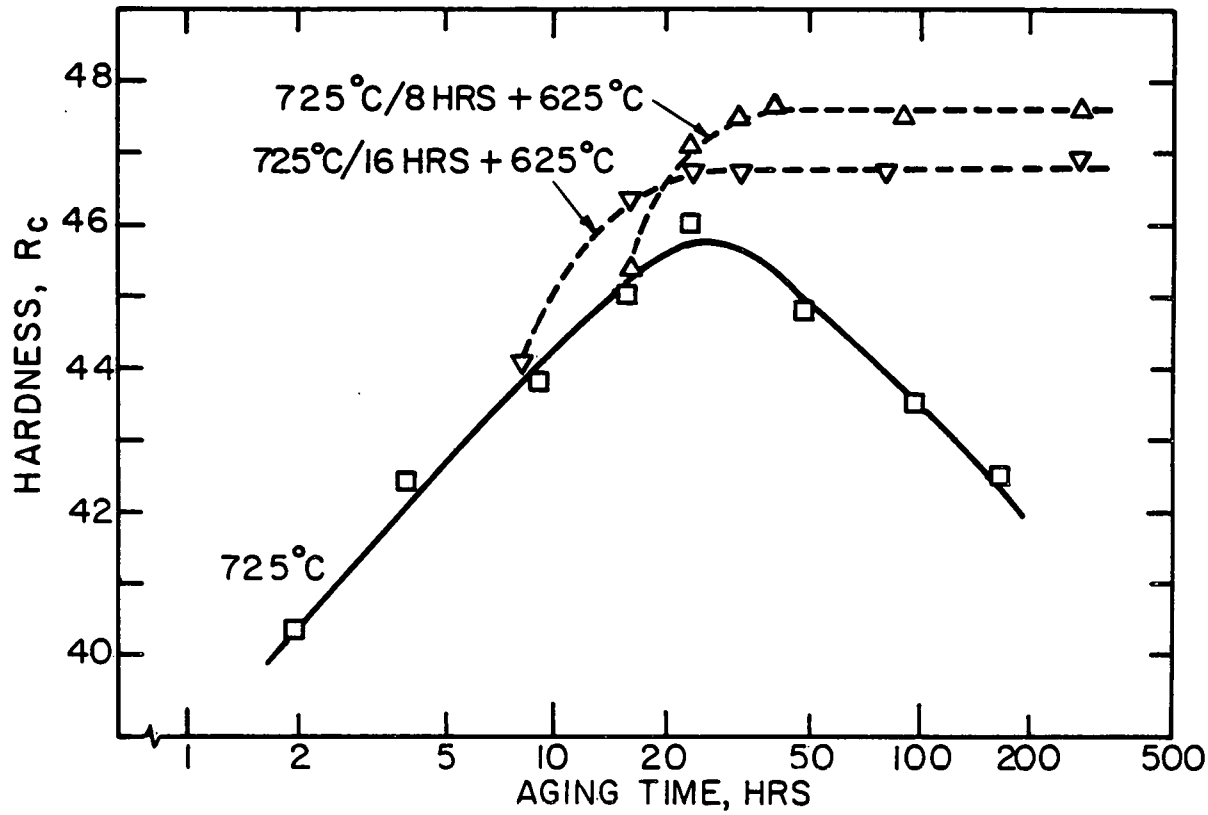

Figure 3

XBL793-5947

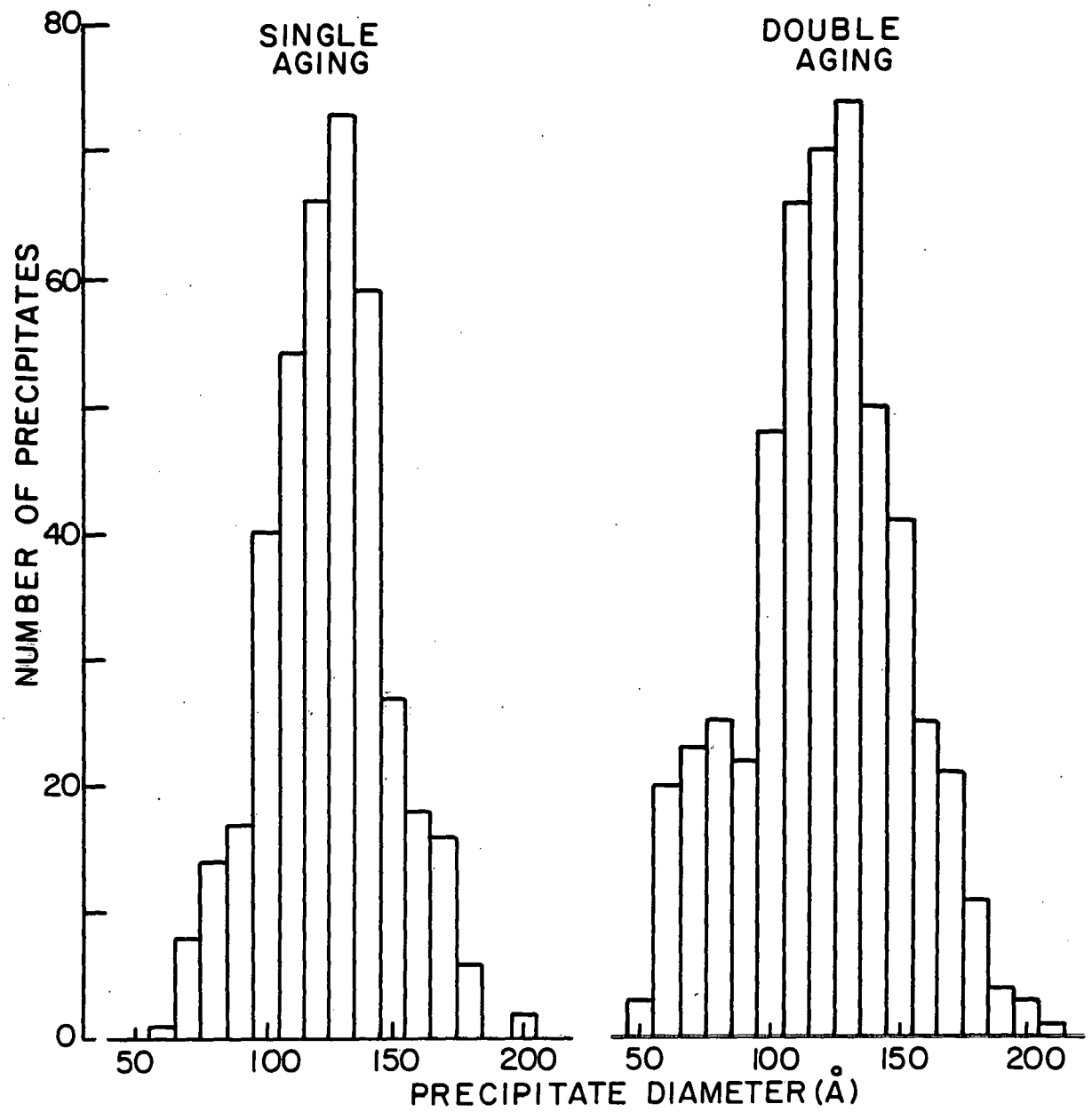

Figure 4

XBL 793-5938

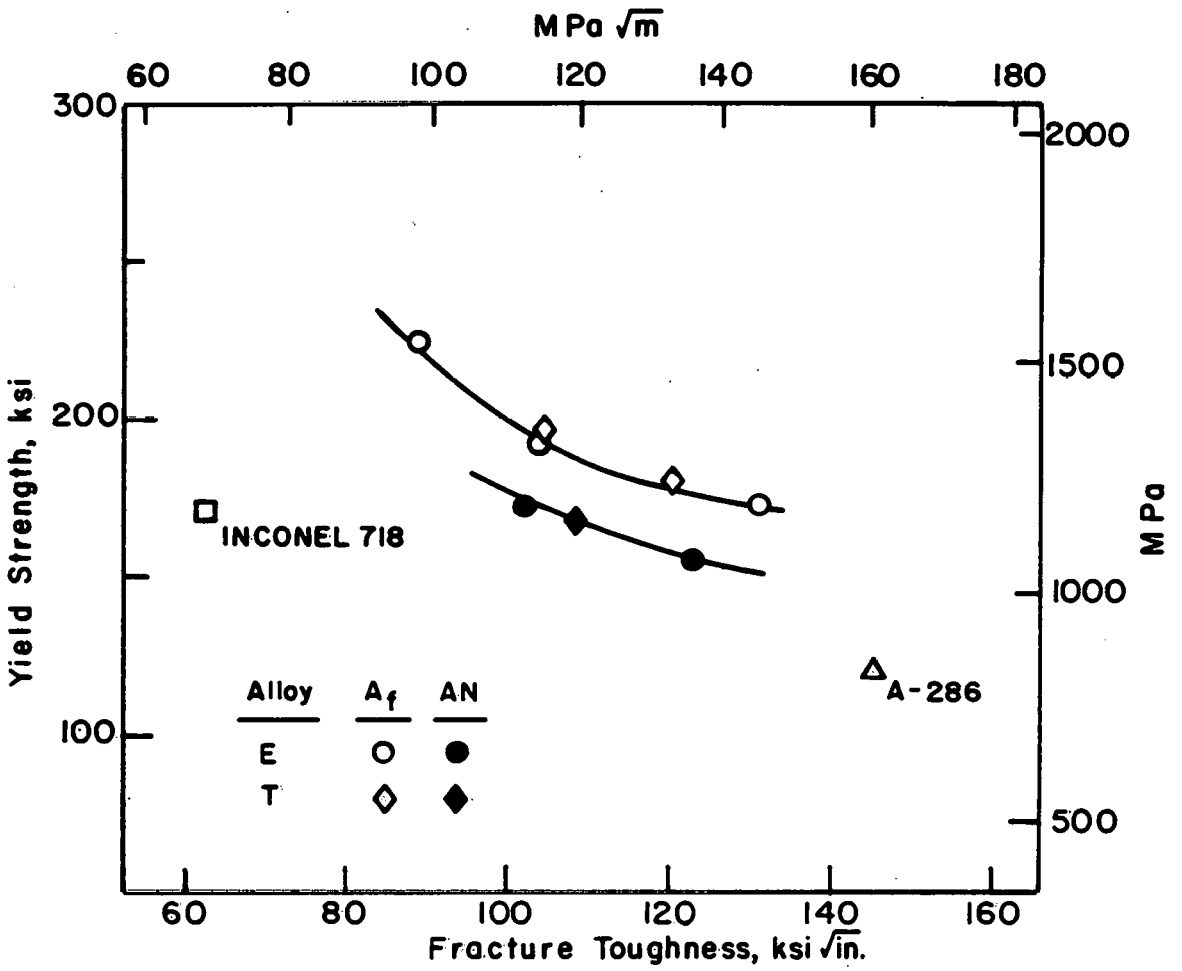

Figure 5

XBL 792-5852A

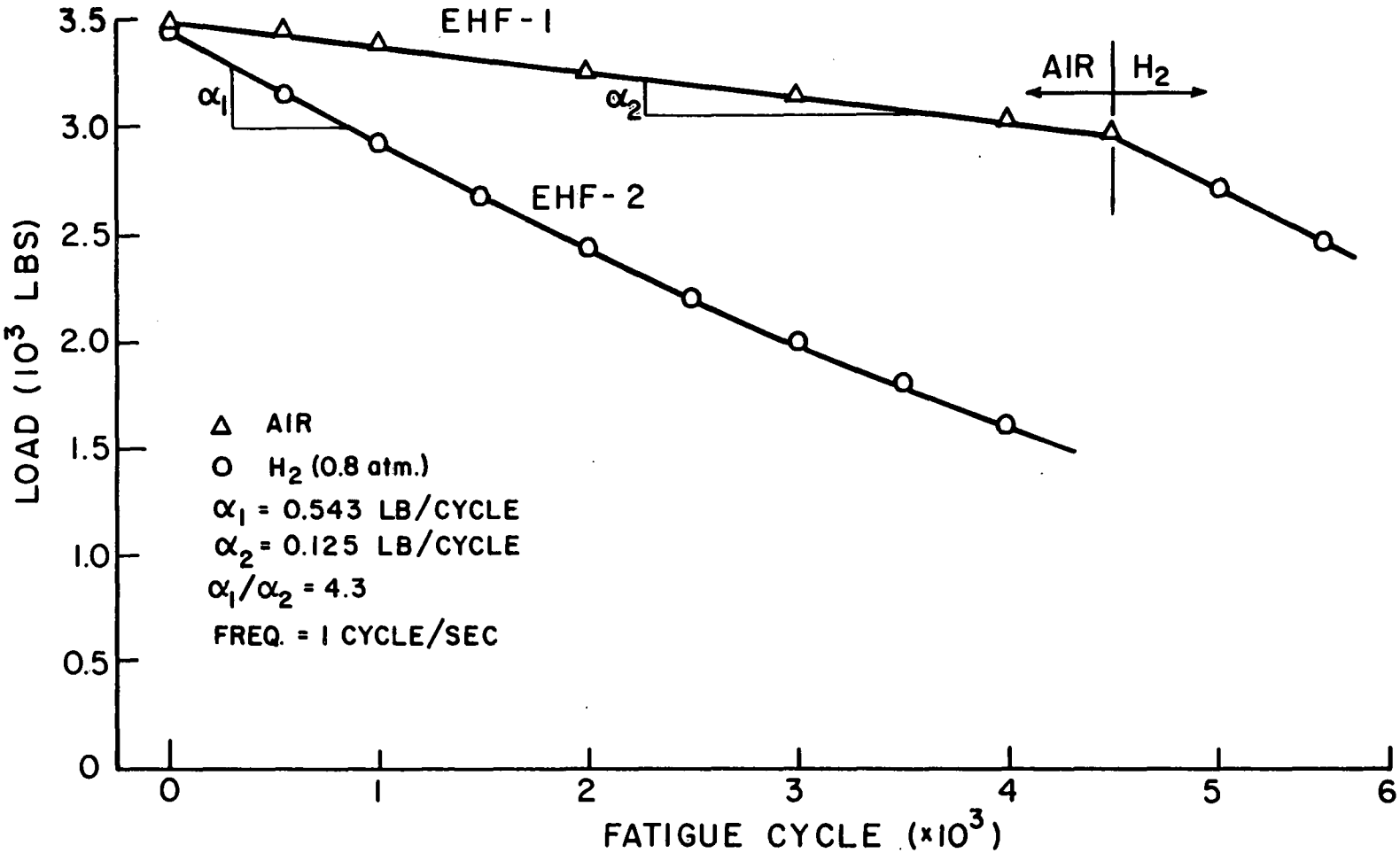

Figure 6

XBL 7811-6200

Alloy E fatigue

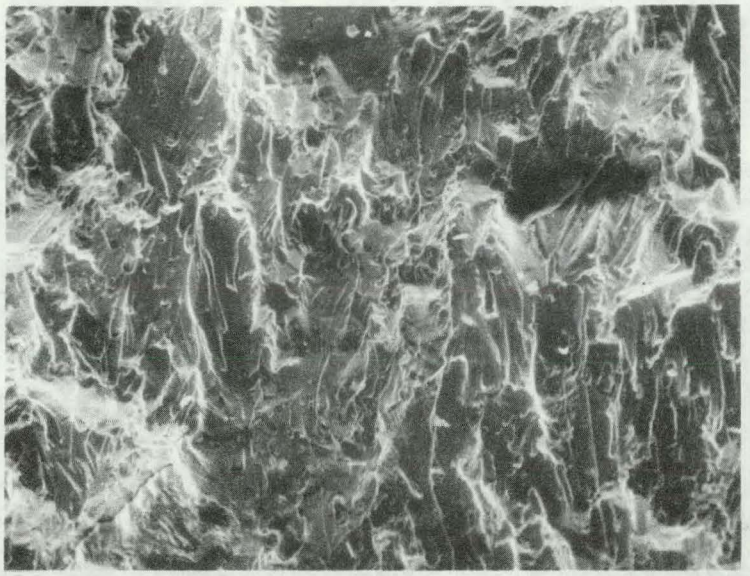

50 μ

in air

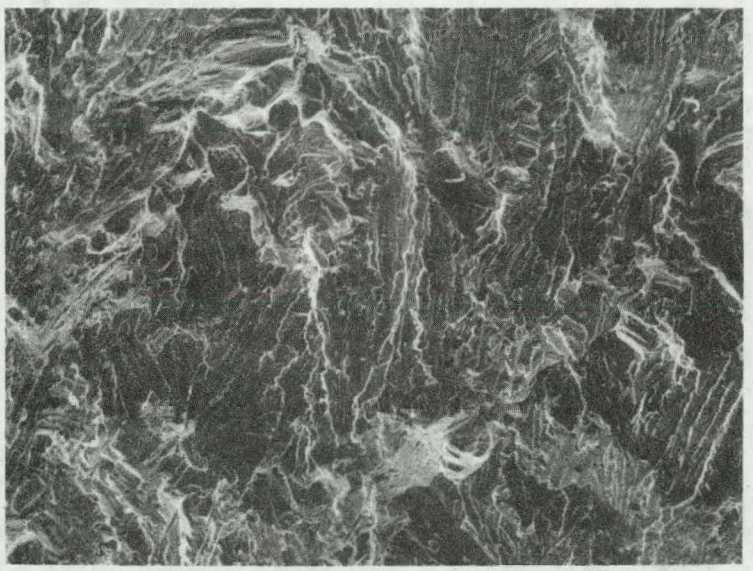

in H_2

Figure 7

XBB 794-5100

Fracture

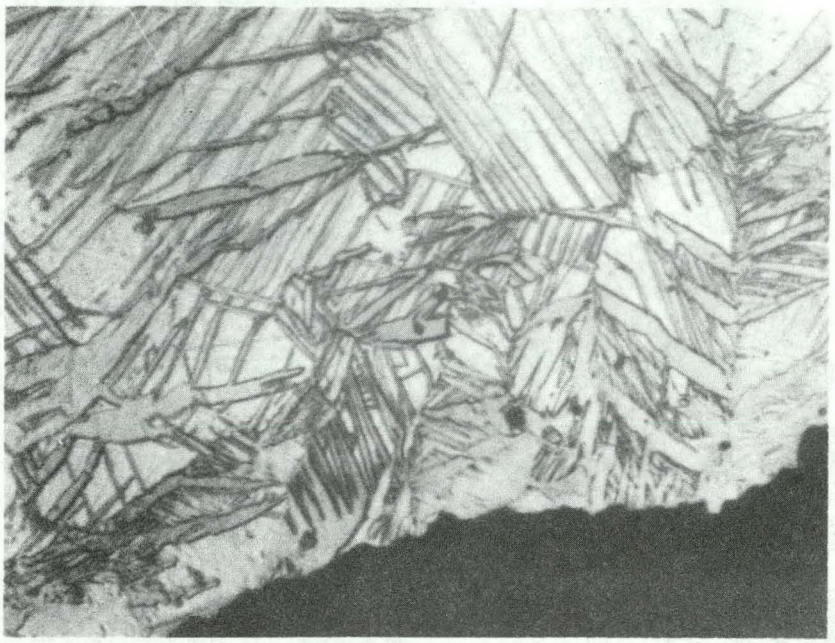

Fatigue

20 μ

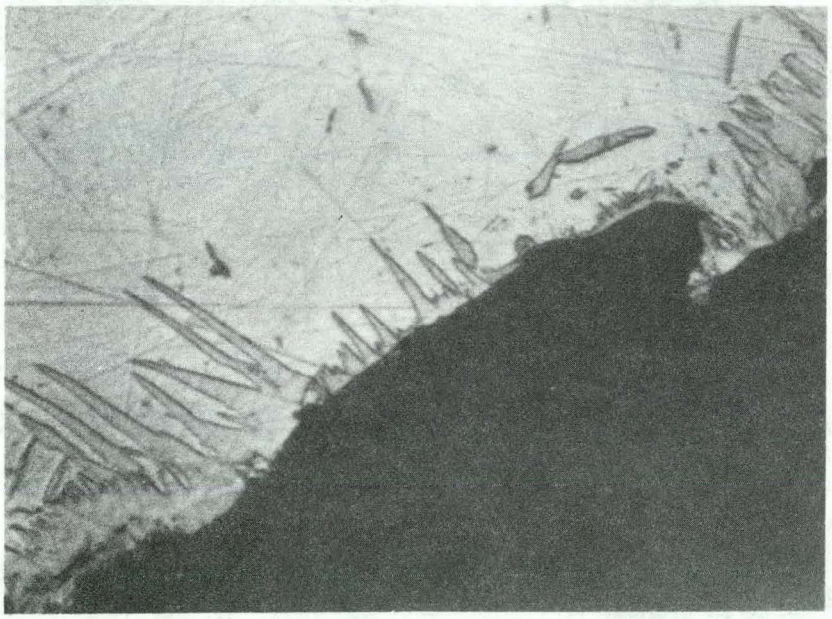

XBB 802-2607

Figure 8

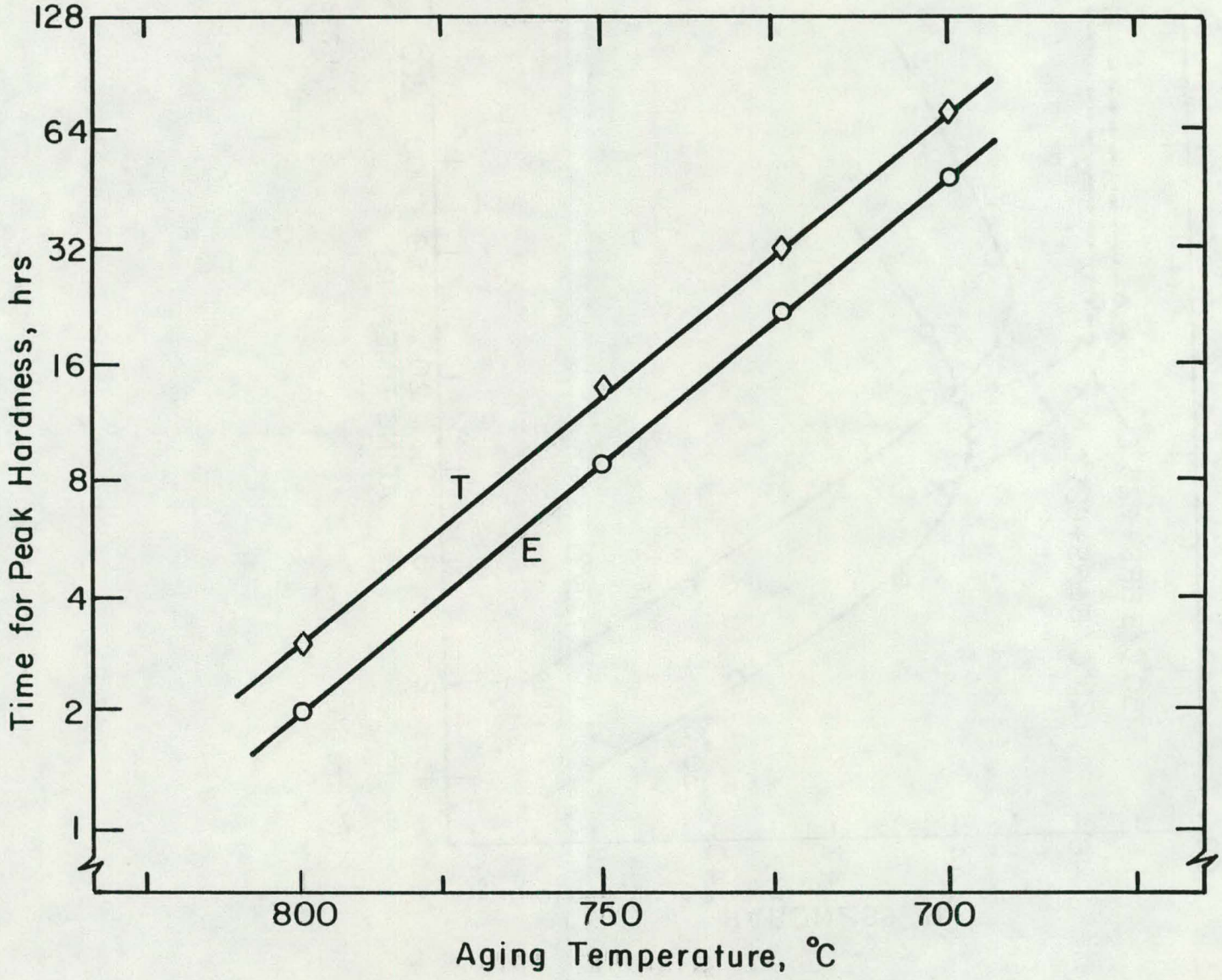

Figure 9

XBL 797-6539

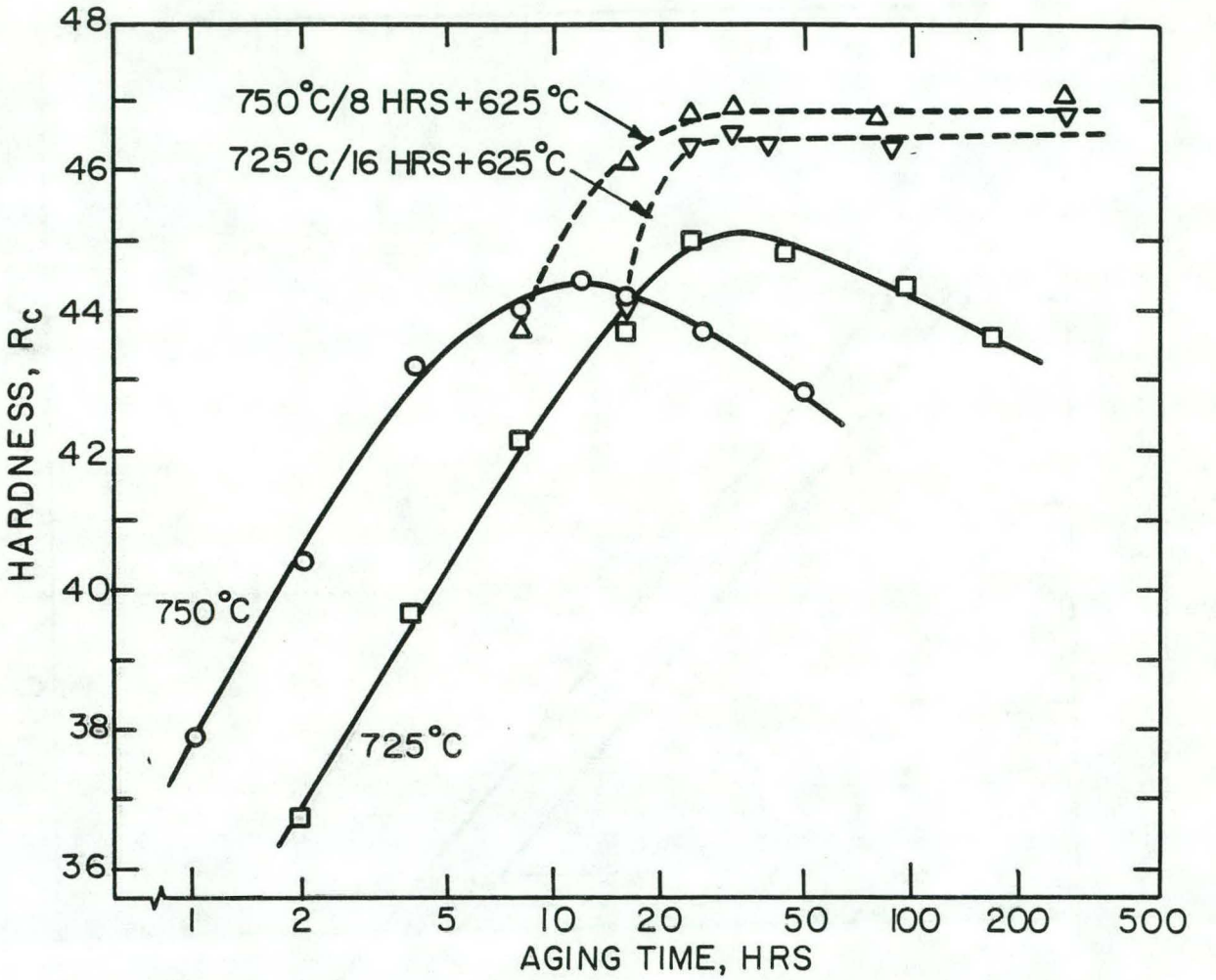

Figure 10

XBL793-5946

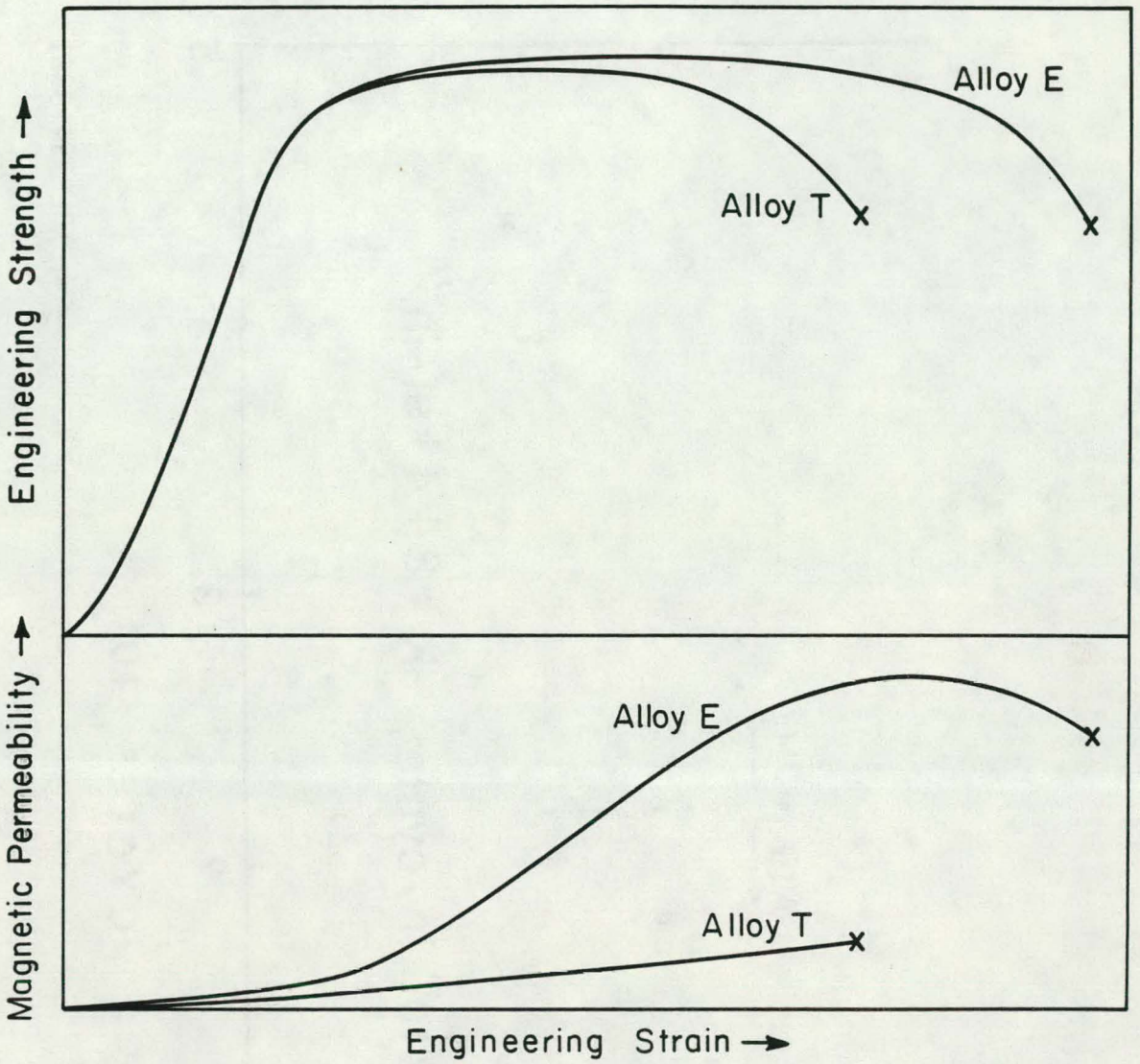

Figure 11

XBL 788-5404

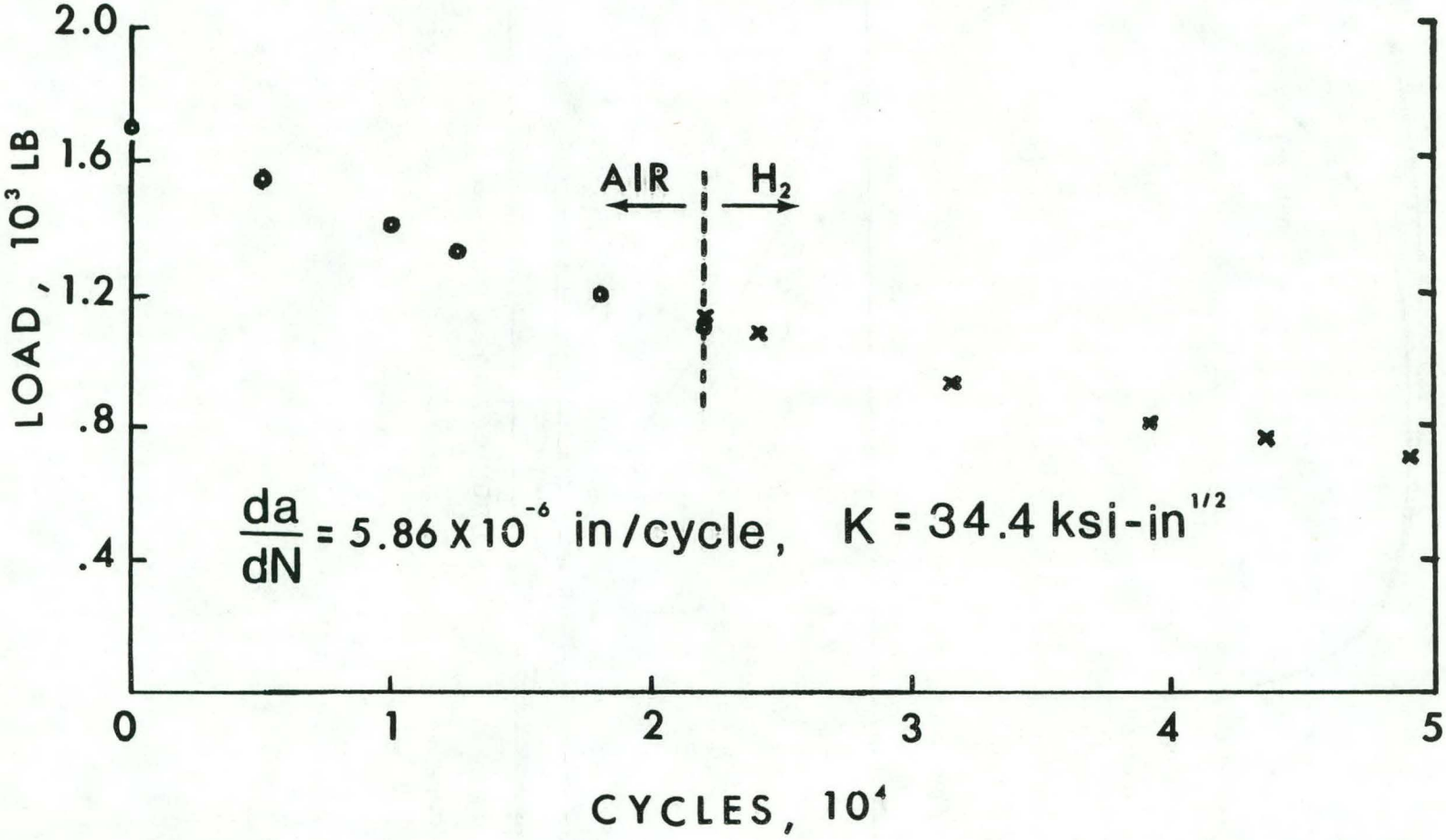

Figure 12

XBL 794-9361

Alloy T fatigue

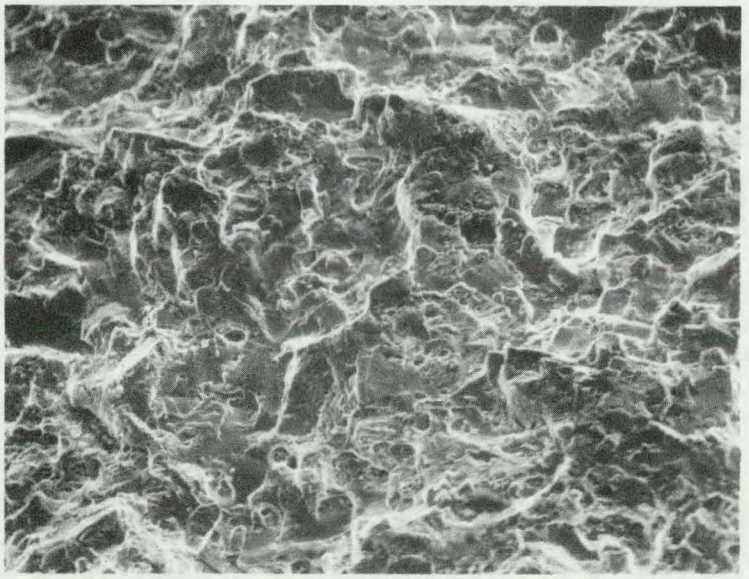

50 μ

in air

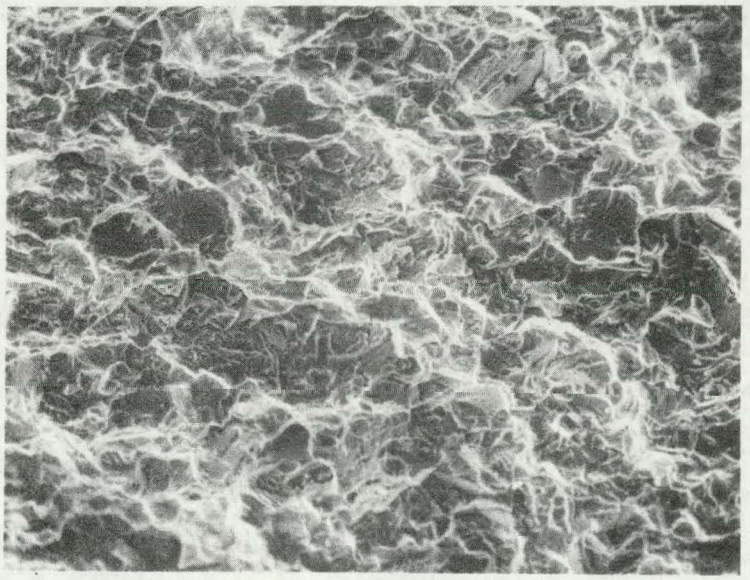

in H_2

Figure 13

XBB 794-5098

TECHNICAL INFORMATION DEPARTMENT
LAWRENCE BERKELEY LABORATORY
UNIVERSITY OF CALIFORNIA
BERKELEY, CALIFORNIA 94720